J|A|C|S
ARTICLES
Published on Web 12/10/2005

Origin of Bulklike Structure and Bond Length Disorder of Pt_{37} and Pt_6Ru_{31} Clusters on Carbon: Comparison of Theory and Experiment

Lin-Lin Wang,[†,‡] Sanjay V. Khare,[†,‡,§] Valeriu Chirita,[||] D. D. Johnson,*[,†,‡] Angus A. Rockett,[†,‡] Anatoly I. Frenkel,[⊥] Nathan H. Mack,[‡,#] and Ralph G. Nuzzo[‡,#]

Contribution from the Department of Materials Science and Engineering, University of Illinois at Urbana-Champaign, 1304 West Green Street, Urbana, Illinois 61801, Frederick Seitz Materials Research Laboratory, 104 South Goodwin Avenue, Urbana, Illinois 61801, Department of Physics and Astronomy, University of Toledo, Toledo, Ohio 43606, Thin Film Physics, IFM, Linköping University, SE-58183 Linköping, Sweden, Department of Physics, Yeshiva University, New York, New York 10016, Department of Chemistry, University of Illinois at Urbana-Champaign, Urbana, Illinois 61801

Received June 13, 2005; E-mail: duanej@uiuc.edu

Abstract: We describe a theoretical analysis of the structures of self-organizing nanoparticles formed by Pt and Ru−Pt on carbon support. The calculations provide insights into the nature of these metal particle systems—ones of current interest for use as the electrocatalytic materials of direct oxidation fuel cells—and clarify complex behaviors noted in earlier experimental studies. With clusters deposited via metallo-organic Pt or $PtRu_5$ complexes, previous experiments [Nashner et al. *J. Am. Chem. Soc.* **1997**, *119*, 7760; Nashner et al. *J. Am. Chem. Soc.* **1998**, *120*, 8093; Frenkel et al. *J. Phys. Chem. B* **2001**, *105*, 12689] showed that the Pt and Pt−Ru based clusters are formed with fcc(111)-stacked cuboctahedral geometry and essentially bulklike metal−metal bond lengths, even for the smallest (few atom) nanoparticles for which the average coordination number is much smaller than that in the bulk, and that Pt in bimetallic [$PtRu_5$] clusters segregates to the ambient surface of the supported nanoparticles. We explain these observations and characterize the cluster structures and bond length distributions using density functional theory calculations with graphite as a model for the support. The present study reveals the origin of the observed metal−metal bond length disorder, distinctively different for each system, and demonstrates the profound consequences that result from the cluster/carbon-support interactions and their key role in the structure and electronic properties of supported metallic nanoparticles.

Introduction

The chemical and topological structures of metallic nanoparticles are key elements that provide the templates that mediate the complex molecular transformations of heterogeneous catalytic processes.[1,2] The interfaces present at the nanoparticle often dictate important properties, ones critical for applications of catalysts in technology. These include such notable issues as their structure and stability (e.g., resistance to sintering[3]), sensitivity to poisoning,[4] the formation of reactive ensembles that lead to selective forms of catalytic transformations,[5] promoter effects,[6] and the control of heat and mass transfer properties. Improving catalysts for important future applications requires significant improvements in our understanding of both their physical and electronic structures. Understanding the factors that most critically serve to control the structures of supported catalytic systems at the nanoscale would constitute a significant advance in the field, one that would directly impact applications. The present theoretical work seeks to provide such insight by examining a set of previously studied nanoscale materials that hold a special utility for fuel cell and catalytic applications.

We have recently synthesized a series of well-defined nanoclusters using metallo-organic complexes.[7−11] The metallic

[†] Department of Materials Science and Engineering, University of Illinois at Urbana-Champaign.
[‡] Frederick Seitz Materials Research Laboratory.
[§] University of Toledo.
[||] Linköping University.
[⊥] Yeshiva University.
[#] Department of Chemistry, University of Illinois at Urbana-Champaign.

(1) Aiken, J. D., III.; Finke, R. G. *J. Mol. Catal. A: Chem.l* **1999**, *145*, 1−44.
(2) Margitfalvi, J. L.; Goboeloes, S. *Catalysis* **2004**, *17*, 1−104.
(3) Min, B. K.; Wallace, W. T.; Goodman, D. W. *J. Phys. Chem. B* **2004**, *108*, 14609−14615.
(4) Seiler, T.; Savinova, E. R.; Friedrich, K. A.; Stimming, U. *Electrochim. Acta* **2004**, *49*, 3927−3936.
(5) Captain, D. K.; Amiridis, M. D. *J. Catal.* **2000**, *194*, 222−232.
(6) Keresszegi, C.; Mallat, T.; Grunwaldt, J.-D.; Baiker, A. *J. Catal.* **2004**, *225*, 138−146.
(7) Nashner, M. S.; Frenkel, A. I.; Adler, D. L.; Shapley, J. R.; Nuzzo, R. G. *J. Am. Chem. Soc.* **1997**, *119*, 7760−7771.
(8) Nashner, M. S.; Frenkel, A. I.; Somerville, D.; Hills, C. W.; Shapley, J. R.; Nuzzo, R. G. *J. Am. Chem. Soc.* **1998**, *120*, 8093−8101.
(9) Hills, C. W.; Nashner, M. S.; Frenkel, A. I.; Shapley, J. R.; Nuzzo, R. G. *Langmuir* **1999**, *15*, 690−700.
(10) Hills, C. W.; Mack, N. H.; Nuzzo, R. G. *J. Phys. Chem. B* **2003**, *107*, 2626−2636.
(11) Frenkel, A. I.; Hills, C. W.; Nuzzo, R. G. *J. Phys. Chem. B* **2001**, *105*, 12689−12703.

nanoclusters of Pt and Pt−Ru prepared in this way were shown to self-organize and form close-packed clusters on high-surface-area carbon supports (Vulcan XC-72). Structural characterizations made of clusters with sizes ranging from 9 to 92 atoms reveal them to be essentially bulklike with fcc(111)-stacked cuboctahedral geometries and, for bimetallic clusters, segregating the Pt atoms preferentially to the ambient (i.e., nonsupport interacting) surfaces of the supported cluster. These structural behaviors are fully studied here using advanced methods of theory and computational modeling.

Many conflicting claims have appeared in the recent literature regarding the structures of metal overlayers and clusters on carbon surfaces. For example, in the case of Ru overlayers deposited on graphite, various forms of data have suggested that growth proceeds via both monolayer[12] and island-based[13] mechanisms—interpretations that are mutually exclusive. Scanning tunneling microscopy experiments that examine the structure of Pt overlayers on graphite found that the growth proceeds via the intermediary two-dimensional islands of Pt in an hcp array,[14] an intriguing observation given our experimental work on cluster growth[8] and the fcc structure of bulk Pt. These selected examples illustrate the range of interesting and frequently contradicting behaviors that are found in the literature on supported-metal model systems, an area that has been developed in several recent comprehensive reviews.[13,15−17]

Here we clarify the nature of the impact that support interactions have on the structures adopted by nanoscale metal clusters and determine the origin for the observed structure of nanoparticles and associated bond length disorder. We compare first-principles, electronic-structure calculations of one representative cluster structure directly with experimentally determined profiles of the bonding present in 37-atom clusters. One can expect different behavior for Pt and mixed Pt−Ru clusters, as Pt (Ru) is at the end (middle) of the transition-metal series, with *d*-levels almost filled for Pt, while half-filled for Ru. Present theoretical studies confirm that Pt and Pt−Ru alloys form incompletely wetting 3D nanoparticles on graphite and provide full profiles of atom-by-atom bond distributions whose natures are not possible to obtain directly from experiment. We directly relate the calculated and experimentally assessed bond length distribution, provide an atomic analysis (structure, electronic charge, and density of states) that reinterprets the experimental data, and helps guide future analysis.

Background on Experiment and Theory. The synthesis and structural characterizations of Pt and Pt−Ru clusters supported on high surface area of carbon black have been described earlier,[7−11] and are summarized here. Bimetallic nanoparticles on carbon were obtained either by the reduction of the neutral molecular carbonyl cluster precursor $PtRu_5C(CO)_{16}$ dispersed on carbon or via reduction of Ru(III) and Pt(II) complexes coimpregnated on the same support phase. In separate experiments, Pt and Ru−Pt clusters were deposited on carbon black via the reduction of single metal source precursors. Detailed structural models of the nanoparticles were deduced from data obtained from in situ extended X-ray absorption fine structure spectroscopy (EXAFS), scanning transmission electron microscopy (STEM), microprobe energy-dispersive X-ray analysis, and electron microdiffraction. These studies showed that nanoparticles obtained from $PtRu_5$ molecular-cluster precursor are exceptionally well-defined materials having a Pt:Ru composition of 1:5, an average diameter of ca. 15 Å, and an oblate (truncated) cuboctahedral structure based upon face-centered-cubic close-packed structure. The supported pure Pt nanoparticles made via the same process also have the same structure. For bimetallic nanoparticles, the local metal coordination environments, as revealed by multiple scattering path analysis of the EXAFS data,[7,8] show that Pt atoms strongly segregate to the ambient surface of the nanoparticles and reside on a Ru-rich core,[7,8] such that Pt atoms form quasi-2D, raft-like structures, presumably to maximize the number of Ru−Ru bonds. Detailed investigations of two representative carbon-supported systems—small bimetallic [$PtRu_5$] clusters of average size and composition, and a carbon-supported pure Pt cluster—showed broad, nonstatistical distributions of metal−metal bond lengths whose averages were close to, but slightly contracted from, values found in the bulk metals. In our previous studies, the polydispersity of the particle sizes, as ascertained by STEM, was small, depending on the system,[7,11] and its effect on the bond length distribution was ruled out even in the larger particles (ca. 40−80 Å).[11] Thus, we associate the enhanced width and the nonstatistical bond length distribution observed in the smallest particles[7,11] solely with the intracluster disorder, rather than the disorder due to ensemble average over the polydispersity.

Thus, due to the observed narrow size distributions, we expect that a single nanocluster already will have bond length disorder that reflects that of the ensemble. Therefore, to make direct comparisons to the distribution of bond lengths of homometallic Pt and bimetallic [$PtRu_5$] nanoclusters deduced from experiment, we simulated Pt_{37} and Pt_6Ru_{31} clusters on graphite with an fcc-(111)-stacked cuboctahedron geometry via full structural minimization. (We note that a calculation of a 37-atom Pt cluster on graphite requires similar number of basis functions and computational intensity as four 800-atom proteins.[18]) The stability of the "segregated" Pt atoms in ambient-surface configuration was verified as being the lowest-energy configuration for Pt_6Ru_{31}/C. Calculations involving carbon were performed on a 7×7 hexagonal, two-dimensional supercell with two atoms per basis to mimic an infinite honeycomb graphite sheet. Separate calculations verified that the use of a single graphite sheet as an approximation for the support did not affect the results while markedly reducing the computational cost.

For the electronic structure calculation, we use density functional theory (DFT) within the local density approximation (LDA), using the exchange−correlation (XC) functional constructed by Ceperley−Alder[19] and parametrized by Perdew and Zunger.[20] We confirmed that the generalized gradient approximation (GGA) to the exchange−correlation, PW91,[21] gave similar structural results in a series of direct, but limited comparisons. As we are primarily interested in structural

(12) Pfandzelter, R.; Steierl, G.; Rau, C. *Phys. Rev. Lett.* **1995**, *74*, 3467−3470.
(13) Binns, C.; Baker, S. H.; Demangeat, C.; Parlebas, J. C. *Surf. Sci. Rep.* **1999**, *34*, 105−170.
(14) Clark, G. W.; Kesmodel, L. L. *J. Vac. Sci. Technol., B* **1993**, *11*, 131−136.
(15) Heiz, U.; Bullock, E. L. *J. Mater. Chem.* **2004**, *14*, 564−577.
(16) Henry, C. R. *Chem. Phys. Solid Surf.* **2003**, *11*, 247−290.
(17) Gates, B. C. *Chem. Rev.* **1995**, *95*, 511−522.
(18) Sugihara, M.; Buss, V.; Entel, P.; Hafner, J.; Bondar, A. N.; Elstner, M.; Frauenheim, T. *Phase Transitions* **2004**, *77*, 31−45.
(19) Ceperley, D. M.; Alder, B. J. *Phys. Rev. Lett.* **1980**, *45*, 566−569.
(20) Perdew, J. P.; Zunger, A. *Phys. Rev. B: Condens. Matter Mater. Phys.* **1981**, *23*, 5048−5079.
(21) Perdew, J. P.; Wang, Y. *Phys. Rev. B* **1992**, *45*, 13244−13249.

parameters, the LDA method was sufficient to develop these correlations; moreover, it is known that in metal solids and at surfaces the GGA does not necessarily give improved results.[22,23]

We utilized a plane-wave basis set, as developed in the Vienna Atomic Simulation Package (VASP),[24−27] with projected augmented wave (PAW) method. A kinetic energy cutoff of 250 eV in the plane-wave basis set was tested for convergence and found sufficient. All calculations were done in a hexagonal supercell of 17.15 × 17.15 × 19.92 Å with periodic boundary conditions. Sufficient surrounding vacuum (at least 12 Å) is included to avoid unphysical interactions among repeating slabs in the *z* direction. The k-point mesh of 2 × 2 × 1 was used. The total energy is converged to 2 meV/atom, and the system is fully relaxed until the absolute force on each atom is smaller than 0.02 eV/Å. Finally, to validate subsequent structural comparisons, we note the VASP−PAW method used is sufficient to reproduce (within the expected 0.5−2.0% error for LDA[28]) the elemental lattice constants of hcp Ru (2.68 Å, 4.24 Å), fcc Pt (3.91 Å), and hexagonal graphite (2.45 Å, 6.69 Å), which compares well with the observed values of (2.71 Å, 4.28 Å),[29] 3.92 Å,[29] and (2.46 Å, 6.71 Å),[30] respectively.

Results and Discussion

As noted, even in nominally Pt-dilute binary phases such as Pt_6Ru_{31}/C, there are nonstatistical distributions of metal−metal (M−M) bonds, which yield bulklike average bond lengths, and there is a strong tendency to segregate Pt to the ambient surface of the cluster. Such outcomes are unique to nanoscale binary clusters of Pt and Ru in several regards. First, although surface segregation occurs in bulk Pt−Ru, the stable structural form at the 1:5 composition of the [$PtRu_5$]-based nanoparticles in the bulk phase diagram remains a mixed alloy−hcp, Ru-rich and fcc, Pt-rich phases−which are exceptionally stable. Clearly, the nanoparticle alloys are too small to support a comparable system of structures. The surface segregation seen in the small clusters is sufficient to deplete the Pt atoms in the core of the clusters. Second, the experimental data indicates a bias to maximize formation of Ru−Ru bonds. Such a bias has not been described in the literature to date. Third, the system (as judged by experiment) tends to prefer bonding between the Ru atoms and the carbon support for bimetallic clusters. Bulk thermodynamics of Pt−Ru alloys cannot resolve such issues. Finally, the clusters formed are oblate, close-packed structures−ones that strongly select habits mirroring the localized geometries of an fcc habit−which is intriguing given that Ru atoms that form the cores of these particles adopt an hcp structure in bulk.

The above discussion highlights a number of complex structural behaviors that are found in supported Pt−Ru nanoparticles, ones that presumably follow from the unique electronic structure of small metal clusters and the consequence of support interactions. Here, from first-principles calculations, we detail the complete explanation of the experimental observations for Pt/C and Pt−Ru/C. Before presenting our results on supported clusters, we make pertinent remarks on bond distributions within *free* metallic clusters that will help guide the interpretation and analysis of the theoretical and experimental results.

Metal−Metal Bonds in Free Clusters. Here we focus on the analysis of metal−metal bond distributions to identify the origin of the bond disorder. To facilitate the discussion, we will refer to the first nearest-neighbor bond between two core atoms, two surface atoms, and a core and surface atom as *core−core*, *surface−surface* (in a nonradial direction around the perimeter of a cluster), and *surface−core* bonds, respectively. For free clusters, we show that surface−surface bonds can be much longer than core−core bonds due to the close packing inside the core, while the shortest bond is always the surface−core in the radial direction, as usually assumed in experimental analyses. For the supported clusters we show that the support-mediated surface−core and surface−surface bonds are responsible for the observed large bond length disorder. Here we contrast free-standing icosohedral (I_h symmetry) and cuboctahedral (O_h symmetry) clusters of Pt_{55} and Ru_{55}, which both have 13-atom core regions, to highlight the effects of symmetry and atom type on the bond distributions within a cluster.

Figure 1 shows the relaxed structures of free 55-atom I_h and O_h Pt and Ru clusters. The relaxed structures are calculated with DFT−LDA in a 20 Å cubic box with at least 12 Å of vacuum and only the Γ point being sampled. The icosahedral cluster is 0.03 and 0.04 eV/atom lower in energy than the cuboctahedral cluster for Pt_{55} and Ru_{55}, respectively. We find that, except for O_h Ru_{55}, the other three clusters all have a nonzero magnetic moment, with 7 μ_B for I_h Ru_{55}, 12 μ_B for I_h Pt_{55}, and 8 μ_B for O_h Pt_{55}. For Pt_{55}, previous DFT−GGA studies[31−33] found that I_h Pt_{55} with 12 μ_B has a lower energy than O_h Pt_{55} with 10 μ_B. For Ru_{55}, a study[34] at the Hatree-Fock level found that O_h Ru_{55} has 0 μ_B. Using DFT−LDA but without relaxing the geometry, Deng et al.[35] found that O_h Ru_{55} with 6 μ_B has lower energy than I_h Ru_{55} with 12 μ_B. Geometry relaxation is important, as shown by our results that the I_h Ru_{55} is actually energetically preferred than O_h Ru_{55}. Such preference is also reported by recent DFT−PW91 studies[36,37] that I_h Ru_{55} with 14 μ_B has lower energy than O_h Ru_{55} with 10 μ_B. We found that, although the magnetic moment of the Ru and Pt cluster is sensitive on XC functional, I_h is preferred over O_h for both Pt_{55} and Ru_{55}, and the discussion on structural analysis does not change when switching from LDA to PW91.

As seen in Figure 1a for the Pt_{55} cluster with I_h symmetry, there are two types of core−core, surface−core, and surface−surface bonds. The core−core bond in the radial (nonradial) direction is 2.57 Å between atoms 1 and 2 (2.71 Å between atoms 2 and 3). The surface−core bond in the radial (nonradial) direction is 2.50 Å between atoms 2 and 4 (2.71 Å between atoms 2 and 5). Finally the surface−surface bond has two

(22) Mattsson, A. E.; Schultz, P. A.; Desjarlais, M. P.; Mattsson, T. R.; Leung, K. *Modell. Simulation Mater. Sci. Eng.* **2005**, *13*, R1−R31.
(23) Kurth, S.; Perdew, J. P.; Blaha, P. *Int. J. Quant. Chem.* **1999**, *75*, 889−909.
(24) Kresse, G.; Hafner, J. *Phys. Rev. B: Condens. Matter Mater. Phys.* **1993**, *47*, 558−561.
(25) Kresse, G. Technische Universität Wien, Ph.D. Thesis, 1993.
(26) Kresse, G.; Furthmüller, J. *Phys. Rev. B: Condens. Matter* **1996**, *54*, 11169−11186.
(27) Kresse, G.; Furthmüller, J. *Comput. Mater. Sci.* **1996**, *6*, 15−50.
(28) Dreizler, R. M.; Gross, E. K. U. *Density Functional Theory: An Approach to the Quantum Many-Body Problem*; Springer-Verlag: New York, 1990.
(29) Kittel, C. *Introduction to Solid State Physics*, 7th ed.; Wiley: New York, 1996.
(30) Yin, M. T.; Cohen, M. L. *Phys. Rev. B* **1984**, *29*, 6996−6998.
(31) Apra, E.; Fortunelli, A. *J. Mol. Struct.-Theochem* **2000**, *501*, 251−259.
(32) Apra, E.; Fortunelli, A. *J. Phys. Chem. A* **2003**, *107*, 2934−2942.
(33) Xiao, L.; Wang, L. C. *J. Phys. Chem. A* **2004**, *108*, 8605−8614.
(34) Guirado-Lopez, R.; Spanjaard, D.; Desjonqueres, M. C.; Aguilera-Granja, F. *J. Magn. Magn. Mater.* **1998**, *186*, 214−222.
(35) Deng, K. M.; Yang, J. L.; Xiao, C. Y.; Wang, K. L. *Phys. Rev. B: Condens. Matter* **1996**, *54*, 2191−2197.
(36) Kumar, V.; Kawazoe, Y. *Eur. Phys. J. D* **2003**, *24*, 81−84.
(37) Zhang, W. Q.; Zhao, H. T.; Wang, L. C. *J. Phys. Chem. B* **2004**, *108*, 2140−2147.

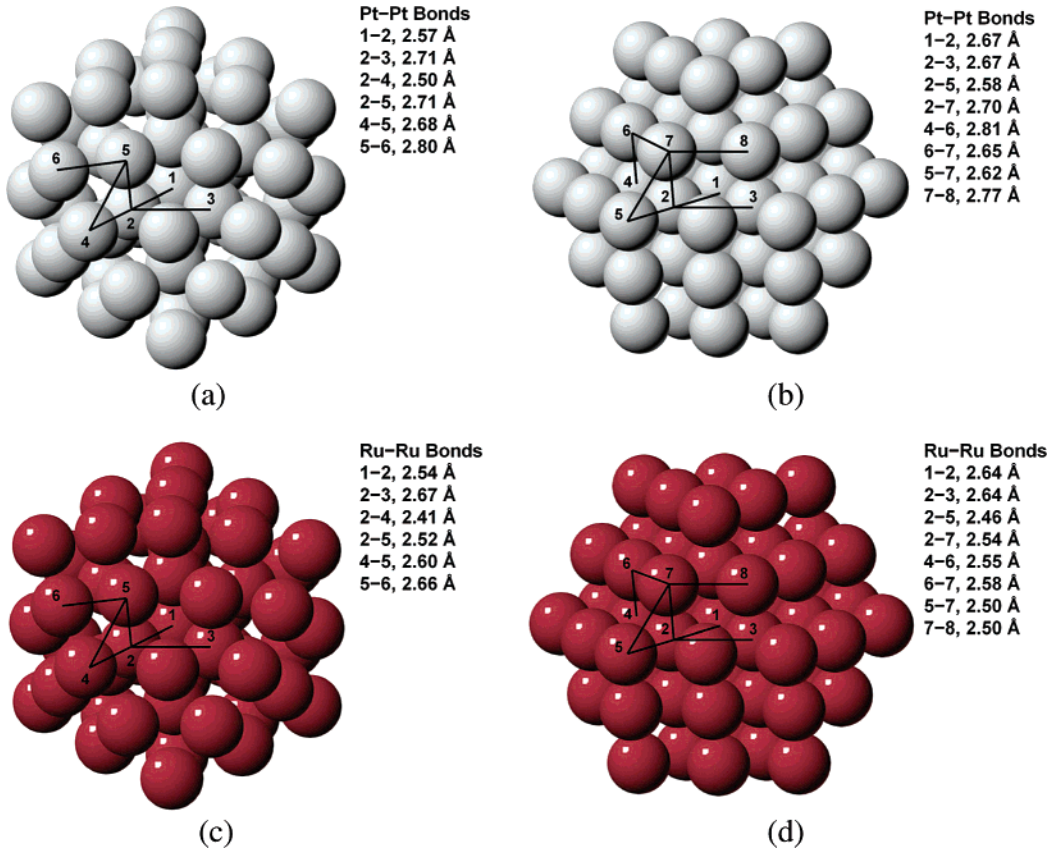

Figure 1. DFT−LDA relaxed structures for a free Pt_{55} cluster with (a) I_h and (b) O_h symmetry, and a Ru_{55} cluster with (c) I_h and (d) O_h symmetry. The light (dark) spheres stand for Pt (Ru) atoms. Metal−metal bonds are indicated in black lines and the corresponding bond lengths are listed. Metal atoms are labeled with numbers and bonds are defined by the two connected atoms. For I_h (O_h) symmetry, the core atoms are 1, 2, and 3 (1, 2, 3, and 4), and surface atoms are 4, 5, and 6 (5, 6, 7, and 8).

nonradial types: 2.68 Å between atoms 4 and 5, and 2.80 Å between atoms 5 and 6. So, the shortest Pt−Pt bond is the radial surface−core bond of 2.50 Å, whereas the surface−surface bond of 2.80 Å is the longest.

For the less stable O_h Pt_{55} seen in Figure 1b, two types of core−core bonds are almost equal at 2.67 Å. There are three types of surface−core bonds: 2.58 Å in the radial direction between atoms 2 and 5, and two nonradial bonds of 2.70 Å between atoms 2 and 7, and 2.81 Å between atoms 4 and 6. Similarly, three types of surface−surface bonds are evident: 2.65 Å between atoms 6 and 7, 2.62 Å between atoms 5 and 7, and 2.77 Å between atoms 7 and 8. Thus, the shortest Pt−Pt bond is the radial surface−core bond of 2.58 Å, and the longest is a nonradial surface−core bond of 2.81 Å.

Clearly then, even for different symmetries, the shortest Pt−Pt bond remains the radial surface−core bond, which is due to the same electronic effect as for the contracted outermost interlayer distance for most semi-infinite metal surfaces. We note that although the outermost interlayer distance for Pt(111) surface is slightly expanded by 1%,[38−40] the curvature of the cluster surface matters. The difference for the longest Pt−Pt bond can be explained from a geometric argument. For the more spherical I_h cluster, the closed-packing of atoms leaves more interatomic space on the surface than in the core region. So the average surface−surface bond tends to be longer than the average core−core bond. For the less spherical O_h cluster, the surface atoms relax toward a spherical shape, especially for the (100) facet, which has more surface area than a (111) facet. The central atom in the (100) facet is relaxed outward and causes the corresponding surface−core bond length to increase, becoming the longest one. The next longest bond is that of the surface−surface bond. This feature of the Pt atoms in the (100) facet relaxing outward to make the O_h Pt_{55} spherical agrees with the study by Apra et al.[31]

As shown in parts c and d of Figure 1, the shortest bond in both I_h and O_h Ru_{55} cluster is again the radial surface−core bond of 2.41 and 2.46 Å, respectively. The longest Ru−Ru bond formed in the I_h Ru_{55} is a nonradial core−core bond of 2.67 Å, slightly larger than the surface−surface bond of 2.66 Å. In the O_h Ru_{55}, the longest bond formed is also a core−core bond of 2.64 Å, but in both nonradial and radial directions. Since the radial core−core bond is much smaller than the nonradial one in I_h Ru_{55}, while both the radial and nonradial core−core bonds are the longest in O_h Ru_{55}, it is evident that the core atoms in the I_h Ru_{55} experience a larger compression than those in O_h Ru_{55}, which agrees well with those found by Jennison et al.[41]

In contrast to Pt_{55}, the core−core bond in Ru_{55} is the longest due to the different electronic structures of Ru and Pt. First, the ratio between the radial surface−core and core−core bond is 0.95 (0.93) for I_h (O_h) Ru_{55}, which is smaller than 0.97 (0.97)

(38) Materer, N.; Starke, U.; Barbieri, A.; Doll, R.; Heinz, K.; Vanhove, M. A.; Somorjai, G. A. *Surf. Sci.* **1995**, *325*, 207−222.
(39) Crljen, Z.; Lazic, P.; Sokcevic, D.; Brako, R. *Phys. Rev. B: Condens. Matter* **2003**, *68*, 195411−195411.
(40) Ho, K. M.; Bohnen, K. P. *Phys. Rev. B* **1985**, *32*, 3446−3450.
(41) Jennison, D. R.; Schultz, P. A.; Sears, M. P. *J. Chem. Phys.* **1997**, *106*, 1856−1862.

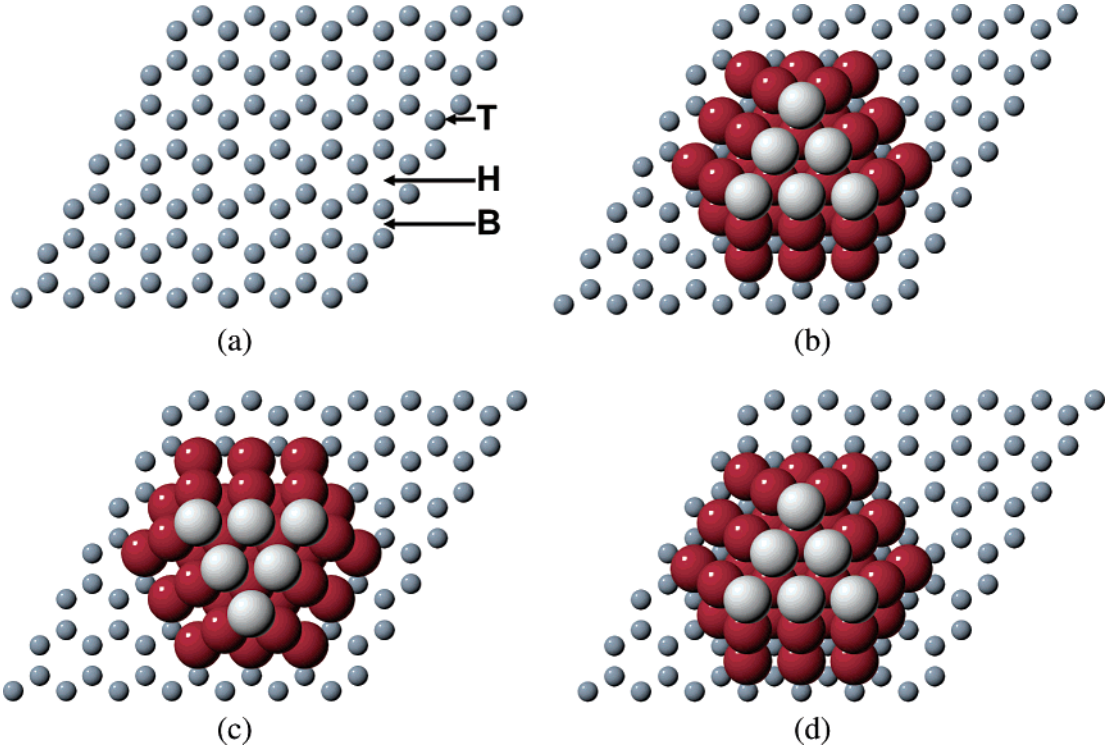

Figure 2. Top view of a bimetallic Pt_6Ru_{31} cluster supported on a graphite surface in a (7 × 7) unit cell. The small dark sphere stands for C atoms, large light (dark) spheres for Pt (Ru) atoms. Part a shows three adsorption sites: T for atop, H for hollow, and B for bridge site. Three configurations with different adsorption sites and orientations are considered: (b) atop, (c) atop-R60 (cluster rotated by 60° with respect to part b), and (d) hollow.

for I_h (O_h) Pt_{55}. So the Ru atom has relatively less space than Pt on the cluster surface. This same feature is reflected in the surface layer relaxation of Ru(0001) and Pt(111) surfaces, where the outermost Ru interlayer distance is reduced by 4%,[42] in contrast to Pt which is expanded only by 1%.[38,39] Second, as Ru has half-filled *d* orbitals, whereas Pt has almost filled *d* orbitals, the Ru−Ru bond is more directional than Pt−Pt bond. The more directional bond results in a less spherical cluster, manifested by less outward relaxation of atoms in the center of (100) facets of Ru cluster than Pt.

Finally, for completeness, for *sp* metals, such as Au clusters, we note that similar features are found as in the bond length distributions of Pt. For example, in an I_h and O_h Au_{55} cluster, the longest bond is a surface−surface bond of 2.91 Å and a nonradial surface−core bond of 2.89 Å, respectively. As reported by Häkkinen et. al,[43] a cuboctahedral Au_{38} cluster calculated using EAM (embedded atom method) shows a core−core bond is the longest; whereas present LDA results (as did ref 43) show that the bonds have a narrower distribution (2.73−2.77 Å). But, in addition, we find that the longest bond is now a surface−surface bond on the (111) facets.

Generally speaking, the radial surface−core bonds are always the shortest; depending on the symmetry and electronic nature of atoms, the longest bond can be surface−surface, surface−core, or core−core bond. However, the first two types of bonds can play a more significant role in the bond length distributions than that of the core−core when the clusters are formed on a substrate because they are in direct contact with the substrate, as we will show later. This fact can have a large impact on the analysis of EXAFS data. Finally, as a particle increases in size from 2 to 100 atoms to 100s to 1000s of atoms, the core−core bonds eventually control the distribution.

Adsorption Configurations and Energies for Supported Clusters. A truncated cuboctahedron cluster with 37 atoms has three atomic layers stacked in the fcc(111) direction, which we refer to as the *z* direction (see Figure 2). The bottom layer has 19 atoms and forms a hexagon, the central layer has 12 atoms, and the top layer has 6 atoms in a triangle. In the perimeter of the bottom hexagon, there are 6 atoms located at the corners. Of the other 6 atoms, 3 of them are in the (111) facet and 3 are in the (100) facet, which we refer to as $M_{(111)}$ and $M_{(100)}$, respectively, with M being either Pt or Ru. In this study, for Pt_{37} and Pt_6Ru_{31} clusters, we consider two high-symmetric adsorption sites on the graphite surface for the starting configuration, atop and hollow sites, as shown in parts b and d of Figure 2. (We considered a number of starting positions for smaller 10-atom clusters to limit search space for the 37-atom cluster, including bridge sites, which always shifted to atop sites.) For atop site, the cluster can have a second configuration formed by rotating the entire cluster 60° along the *z* axis (we refer to this as atop-R60), as shown in Figure 2c. Initially, we put each of the 19 metal atoms in the bottom layer of the clusters on the same type of site and stack the other two atomic layers accordingly. We then use geometry optimization to let the system relax to its equilibrium.

Some previous theoretical studies suggest that a Ru overlayer on graphite can be magnetic if the overlayer is kept above the equilibrium height.[44] Nonetheless, magnetism is lost via a first-order collapse for a smaller height of the overlayer, with

(42) Mannstadt, W. *Surf. Sci.* **2003**, *525*, 119−125.
(43) Häkkinen, H.; Barnett, R. N.; Landman, U. *Phys. Rev. Lett.* **1999**, *82*, 3264−3267.
(44) Hergert, W.; Rennert, P.; Demangeat, C.; Dreysse, H. *Surf. Rev. Lett.* **1995**, *2*, 203−217.

Table 1. DFT−LDA Adsorption Energies (eV) for a Pt_{37} and Pt_6Ru_{31} Nanocluster Supported on a Graphite Surface for Atop, Atop-R60, and Hollow, as Shown in Figure 2

nanocluster	atop	atop-R60	hollow
Pt_{37}/C(0001)	2.69	2.32	2.59
Pt_6Ru_{31}/C(0001)	8.39	8.15	6.25

equilibrium being nonmagnetic. As for nanoclusters, magnetic structures are expected, especially in free clusters, as seen in the previous section. However, for intermediate-sized nanoclusters, magnetic structures are less likely to be formed in supported clusters as for similar reasoning for the collapse of magnetism in supported Ru overlayers.[13,44] In our calculations, we find that the carbon-supported Pt_6Ru_{31} and Pt_{37} clusters are indeed nonmagnetic.

The adsorption energies of the three different initial configurations for both Pt_{37} and Pt_6Ru_{31} clusters are listed in Table 1. For the Pt_{37} cluster, the adsorption energies show that atop is preferred by at least 0.10 eV to hollow and 0.37 eV to atop-R60. For the Pt_6Ru_{31} cluster, atop is preferred by at least 0.24 eV to atop-R60 and 2.14 eV to hollow. Clearly, the atop site is energetically preferred for both clusters. For both Pt and Pt−Ru, the similar adsorption energies for the atop and atop-R60 configurations arise from the fact that the bottom layer in contact with support has very similar electronic interactions. Regardless of the different adsorption sites, the bimetallic Pt_6Ru_{31} cluster with Ru on the bottom layer has much larger adsorption energies than the homometallic Pt_{37} cluster. This shows that Ru has stronger interaction with the carbon support than Pt does. The different strength of interaction with carbon is determined by the difference in the filling of the metal *d* orbitals, since Ru has a half-filled *d* orbital, while Pt has an almost filled *d* orbital. Configurations with Pt sandwiched internally to the supported Pt_6Ru_{31} cluster are at least 4 eV higher than the surface-segregated Pt configuration. Because both the supported Pt_{37} and Pt_6Ru_{31} clusters are the energetically most stable with the configuration starting from the atop site, we concentrate on the structural analysis of this configuration for the remainder of this discussion.

As the result of the relaxation, the bottom hexagon is not commensurate with the graphite surface anymore. The metal atoms in the bottom layer can relax toward different adsorption sites nearby. Due to the interaction between the substrate and cluster, an *intra*layer buckling is induced in both the graphite surface and the atomic layers of the clusters. In Figure 3, the intralayer buckling together with the interlayer distances are shown schematically. For the Pt_{37}/C(0001) system, as seen in Figure 3a, the supporting graphite surface evidences a buckling of 1.30 Å. The buckling is 0.55 Å in the bottom Pt layer, 0.23 Å in the central Pt layer, and 0.07 Å in the top Pt layer, respectively. This shows that the structure modification inside the Pt_{37} cluster is the largest in the bottom Pt layer (which is in direct contact with the carbon substrate), and that this modification is effectively screened by the electrons to make the top Pt layer almost flat. The adsorption distance for the Pt_{37} cluster supported on the graphite surface is 2.34 Å, which is calculated as the difference between the average position of the bottom Pt layer and that of the carbon atoms in the *z* direction. The interlayer distance in the cluster can be calculated in a similar way. The interlayer distance between the central and bottom Pt layers is 2.22 Å, and that between the top and central Pt layers

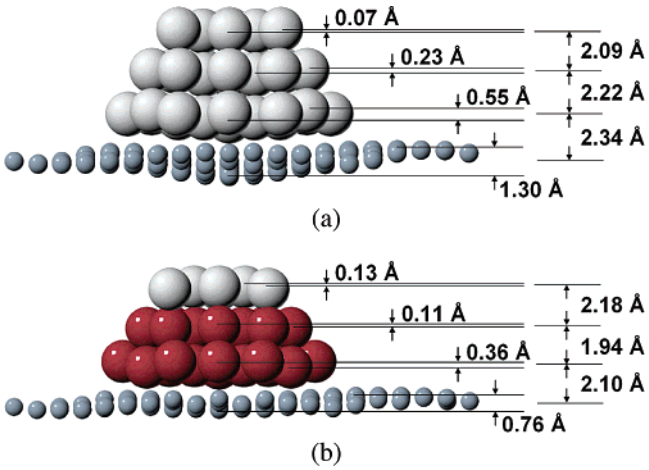

Figure 3. Side view of the relaxed structures calculated with DFT−LDA for (a) Pt_{37} and (b) Pt_6Ru_{31} clusters supported on a graphite surface. The legends are the same as in Figure 2. In each panel, both the intralayer buckling and interlayer distances are listed.

is 2.09 Å. For the Pt_6Ru_{31}/C(0001) system, the buckling deduced from the calculations is 0.76 Å in the graphite surface, 0.36 Å in the bottom Ru layer, 0.11 Å in the central Ru layer, and 0.13 Å in the top Pt layer, respectively. Again, the effect of buckling is diminished in going from the bottom to the top metal layer. The adsorption distance is 2.10 Å, the interlayer distance is 1.94 Å between the bottom Ru and central Ru layers, and 2.18 Å (largest) between the central Ru and top Pt layers. The smaller adsorption distance as a result of the larger binding energy for the mixed cluster than the pure Pt cluster indicates that the Ru−C interaction is stronger than the Pt−C interaction. The Ru−Ru interlayer distance is smaller than the Pt−Pt and Pt−Ru interlayer distance, which is understandable, considering that Pt has a larger lattice constant than Ru (as would be inferred from the different atomic radii of Ru and Pt).

A closer look at Figure 3 shows that the buckling in the bottom Ru and Pt layer is different in each case. In this side view of the supported clusters, we see that one (100) facet is in the center with a square shape and two (111) facets are on the side each with a triangular shape. As seen in Figure 3a, the $Pt_{(111)}$ atoms have the highest position in the *z* direction in the bottom Pt layer, which determines the magnitude of the buckling. In contrast, the buckling in the bottom Ru layer, as shown in Figure 3b, is determined by the lowest position of $Ru_{(111)}$ atoms in the *z* direction. These different behaviors in the relaxation of the $M_{(111)}$ atoms for Pt and Ru have a large impact on the metal−metal bond disorder, which we will discuss in detail in the next section.

Metal−Metal Bond Length Distribution Analysis: Theory vs Experiment. EXAFS is often used to probe the local coordination environment of an atom in a nanoscale metal cluster. Using the latest advances in EXAFS theory,[45] ones that take into account multiple-scattering and non-Gaussian bond-length disorder, a theoretical EXAFS spectrum can be generated for essentially any model cluster. The experimental EXAFS signal is then fitted with a theoretical simulation, and the structural parameters are varied until the best agreement is found between the data and theory. For a converged structural model, the local coordination numbers, metal−metal bond lengths, and

(45) Rehr, J. J.; Albers, R. C. *Rev. Mod. Phys.* **2000**, *72*, 621−654.

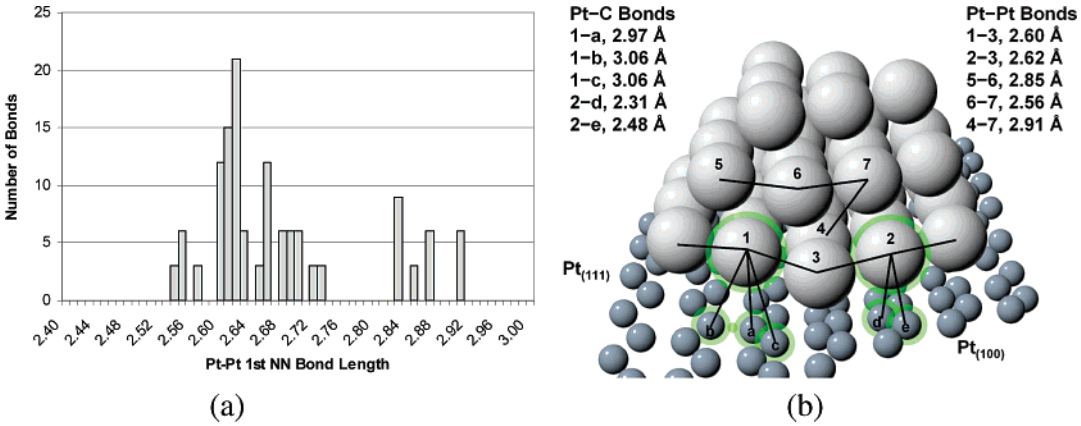

Figure 4. (a) Distribution of first NN Pt−Pt bond lengths calculated with DFT−LDA for relaxed Pt_{37} cluster supported on a graphite surface. The average first NN Pt−Pt bond length is 2.68 Å. The relaxed structure is shown in part b. The legends are the same as in Figure 2. Significant metal−carbon and metal−metal bonds are drawn in black lines, and the corresponding bond lengths are listed. Each bond is defined by the two connected atoms. Metal and carbon atoms are labeled in numbers and letters, respectively. The Pt $_{(111)}$, $Pt_{(100)}$ atoms and the closest C atoms to them are highlighted.

bond-length disorder parameters are then determined, and the uncertainties in the results are evaluated. Previously, we have used this method and the UWXAFS data analysis package[46] to characterize the metal−metal bond lengths for both homometallic Pt and bimetallic Pt−Ru nanoclusters supported on carbon.[7−9,11]

Using the present DFT calculations, we can make a direct comparison between experiment and theory and provide new insights as to how the structure of the metal cluster is relaxed in the presence of the carbon support. A detailed atom-by-atom description of the metal−metal bonding present in the supported metal nanocluster is a level of structural understanding that is typically inaccessible to experiment, yet are readily accessible via theory-guided modeling. In this section, we will focus on the metal−metal bond length distributions calculated from DFT and compare them to the experimental EXAFS data.[7,11] An analysis is made to identify the origin of the significant contributions to the bond disorder from some specific bonds.

Pt_{37} Cluster. In Figure 4, we present the calculated bond length distribution and a description of the relaxed structure for a Pt_{37} cluster supported on a graphite surface at zero Kelvin ($T = 0$ K). DFT−LDA yields 2.68 Å as the average first nearest neighbor (NN) Pt−Pt bond length. From EXAFS data analysis[11] of the smallest (17 Å in diameter) Pt/C nanoclusters measured at room temperature ($T = 300$ K), the experimental 1NN Pt−Pt bond length is 2.756(3) Å.[11] The DFT−LDA ($T = 0$ K) value is less than 3% smaller than the EXAFS value, but note that the average bond length from DFT (expected to be smaller than experiment due to LDA error) will increase with temperature due to the large bond disorder (see below). Comparing the EXAFS value to the bulk first NN Pt−Pt bond length of 2.76 Å, the supported Pt_{37} cluster already has a bulklike average bond. In our calculation, the second, third, and fourth NN Pt−Pt bond lengths are found to be 3.72, 4.61, and 5.25 Å, respectively.

Figure 4a shows the atom-by-atom DFT−LDA calculated distribution of the first NN bond lengths for Pt−Pt in the graphite-supported Pt_{37} cluster. The Pt−Pt bond length has a broad distribution from 2.55 to 2.91 Å, corresponding to −5% and +9% change of the LDA average value of 2.68 Å, respectively. The magnitude of the bond length disorder is quite large, as found experimentally and discussed below. More surprisingly, the bond length distribution is bimodal. Although most of the Pt−Pt bond lengths are shorter than 2.76 Å, there are some Pt−Pt bond lengths longer than 2.84 Å, and there are no bond lengths between, see Figure 4a. The longer bonds contribute significantly to the calculated T = 0 K average value of 2.68 Å.

Experimentally, the bond length disorder can be quantified as the standard deviation (σ^2) of the bond length. From their temperature-dependent EXAFS study of bond lengths in the smallest (17 Å diameter) Pt/C nanoclusters, Frenkel et al.[11] deduced a significant (0.0017(2) Å^2) contribution of the static, configurational disorder to the σ^2 of the data. To understand the origin of this structural disorder experimentally, a simple model of surface relaxation was constructed using a universal force field that assumed radial, isotropic bonds for core atoms having one fixed bond length and surface−core bonds having a statistical distribution. It was found that a broad and, notably, bimodal distribution was needed to fit both the average Pt−Pt bond length and the static component of the σ^2 parameter determined from experiments. The bond length distribution showed significant contributions from substantially larger bond length. This bimodal distribution of bond lengths agrees very well with the present DFT results for Pt_{37}/C and is expected to hold true for larger Pt clusters as well. It is remarkable that such a simple ad hoc model produces the same quantitative aspects in the inferred distribution as does the DFT results.

Importantly, the longest M−M bonds in the simple model used in the EXAFS analysis correspond to those of core−core bonds. However, as noted earlier, the core−core bonds are not necessarily the longest. The correct identity depends on both the type of atoms present and the symmetry of the cluster. From our detailed first-principles results, we find that the precise origin of the large bond length disorder is due to the combined effects of the anisotropic relaxations within the carbon-supported clusters and the interaction of the bottom layer of metal atoms with the carbon support (i.e., interfacial interactions).

Figure 4b shows the nature of some of the significant perturbations of the first NN Pt−Pt and Pt−C bond lengths found in the relaxed Pt_{37} cluster supported on the graphite surface. Along the perimeter of the bottom hexagon, the Pt−Pt bond length in the (111) facet is 2.60 Å and that in the (100)

(46) Stern, E. A.; Newville, M.; Ravel, B.; Yacoby, Y.; Haskel, D. *Physica B* **1995**, *209*, 117−120.

Table 2. Average Bond Lengths from EXAFS, LDA, and PW91 for Supported [PtRu5] Clusters[a]

	Pt–Pt			Pt–Ru			Ru–Ru		
NN shell	EXAFS	LDA	PW91	EXAFS	LDA	PW91	EXAFS	LDA	PW91
1	2.69(3)	2.67	2.74	2.70(1)	2.64	2.69	2.67(1)	2.56	2.60
2	3.78(3)			3.79(2)	3.71	3.79	3.78(1)	3.57	3.63
3	4.66(4)	4.62	4.75	4.70(2)	4.52	4.61	4.68(1)	4.48	4.55
4	5.38(3)	5.28	5.42	5.40(1)	5.13	5.22	5.42(2)	5.20	5.28

[a] Bond lengths (Å) per NN shell for Pt−Ru clusters on C are reported in the same assignment used in ref 7, where the NN shells are defined on an fcc lattice (see Figure 5). Pt−Pt second NN bond is not present in Pt_6Ru_{31} due to Pt segregation to the uppermost (third layer) of the supported cluster. Experimental bond lengths (ref 7) were obtained via analysis of EXAFS data on the truncated cuboctahedral structure. Theoretical data are the average bond lengths calculated for a Pt6Ru31 cluster supported on a graphite surface using LDA and PW91.

facet is 2.62 Å. While these bond lengths are almost the same, the positions of the $Pt_{(111)}$ and $Pt_{(100)}$ atoms in the *z* direction are in fact quite different. As mentioned above, the $Pt_{(111)}$ atoms tend to relax upward and have the highest position among the bottom Pt layer. The upward movement of the $Pt_{(111)}$ induces strain and pushes atoms 5 and 6 in the central Pt layer apart, as indicated by the long Pt−Pt bond of 2.85 Å between them. This effect also results in the shortest Pt−Pt bond of 2.56 Å between atoms 6 and 7 in the neighboring (100) facet in the central Pt layer. The longest Pt−Pt bond of 2.91 Å is between atom 7 in the center of the (100) facet and atom 4 in the bottom layer. Unlike $Pt_{(111)}$ atoms, $Pt_{(100)}$ atoms remain in the same level as the other Pt atoms (3 and 4) in the bottom layer. In contrast, the Pt−Pt bond between two core Pt atoms in the central layer is 2.67 Å (not shown in the figure). So the longest Pt−Pt bonds in the supported cluster are not among the core−core atoms or surface−surface atoms but between surface Pt atoms in the central layer and Pt atoms in direct contact with the substrate: these are interlayer bonds.

The different relaxation between the $Pt_{(111)}$ and $Pt_{(100)}$ atoms can be related to the local adsorption environment. Initially, both the $Pt_{(111)}$ and $Pt_{(100)}$ atoms adsorb on the atop site. Due to expansion of the cluster during the relaxation, the $Pt_{(111)}$ atoms are pushed toward the nearby hollow sites, while the $Pt_{(100)}$ atoms are pushed toward the nearby bridge sites. After the relaxation, as seen in Figure 4b, the $Pt_{(111)}$ atom has three closest carbon atoms with one at 2.97 Å and two at 3.06 Å around the hollow site, while the $Pt_{(100)}$ atom has two closest carbon atoms with one at 2.31 Å and one at 2.48 Å around the bridge site. As indicated by the Pt−C bond lengths, the $Pt_{(111)}$ atom has weaker interactions with the carbon support than the $Pt_{(100)}$ atom. This shows that the Pt atoms prefer to adsorb on the bridge over the hollow site on the graphite surface.

Pt_6Ru_{31} Cluster. A similar analysis of bond length distributions was made for the Pt_6Ru_{31} cluster supported on a graphite surface. The shell-wise average bond lengths calculated with LDA and GGA, along with those deduced from EXAFS experiments[7] for supported [PtRu5] clusters, are listed in Table 2. When studying Table 2, one notes that the bonds determined from the EXAFS data are geometric, e.g., the fourth nearest-neighbor bond is twice that of the nearest-neighbor within the uncertainties, as expected or an fcc lattice, (see Figure 5). For the first nearest neighbor bond lengths, the experimental data are 2.69 ± 0.03 Å for Pt−Pt, 2.70 ± 0.01 Å for Pt−Ru, and 2.67 ± 0.01 Å for Ru−Ru, respectively, which have a difference

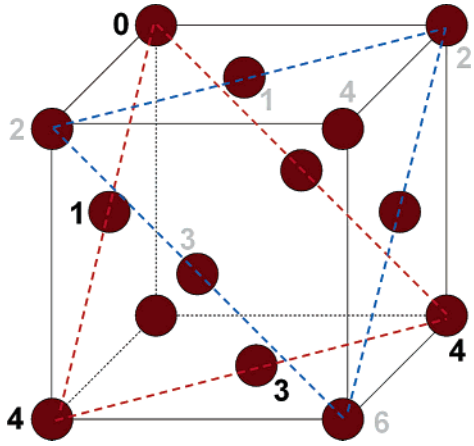

Figure 5. Assignment of NN shell bond lengths defined on an ideal fcc lattice as listed in Table 2. Two consecutively stacked (111) planes are highlighted in red and blue. The black (gray) numbers labeled on the atoms indicate the in-plane (out-plane) *n*th shell that the atoms are in with respect to the atom 0. The 5th NN shell is in the face of next cube, which is not shown.

of less than 3% from the bulk values.[47] The DFT−LDA calculated first NN bond lengths of 2.67 Å for Pt−Pt, 2.64 Å for Pt−Ru, and 2.56 Å for Ru−Ru also have a difference of less than 3% from the theoretical bulk values. For the higher NN shells, the bond lengths calculated from DFT−LDA compare well with the experimental data. GGA(PW91) calculations only slightly improves the Pt−Ru and Ru−Ru bond lengths, but it overestimates the Pt−Pt first NN bond length. See Table 2.

As a general trend found in the theoretical data, we found that the Pt−Pt bonds in different NN shells are always the longest among the three, followed by Pt−Ru, then Ru−Ru bonds. Although the experimental data cited[7] shows that the Pt−Ru bond lengths are the largest, they overlap with the Pt−Pt bond lengths within the experimental uncertainties. A more recent experimental paper[8] with smaller uncertainties shows that the first NN Pt−Pt bonds are always longer than Pt−Ru bonds for a wide range of temperatures, which agrees with the trend seen in our DFT calculations.

Figure 6 shows the distribution of the first NN bond lengths for Pt−Pt in part a, Pt−Ru in part b, and Ru−Ru in part c, respectively. The Ru−Ru bond length has a broad distribution from 2.36 to 2.82 Å as seen in Figure 6c, which corresponds to about ±10% change with respect to the average LDA value of 2.56 Å. The magnitude of the bond disorder found in the calculations is as large as that seen for the supported Pt_{37} cluster. Most of the Ru−Ru bond lengths are shorter than 2.70 Å; however, there are several Ru−Ru bond lengths of 2.82 Å, which are even longer than the largest Pt−Pt or Pt−Ru bond lengths of 2.76 Å, as seen in Figure 6a,b.

As shown in Figure 6d, both the shortest and longest Ru−Ru bonds are from the perimeter of the bottom hexagon, which is in direct contact with the graphite: these are intralayer bonds (in contrast to pure Pt cluster, where bond disorder arose via interlayer bonds). Three of them are 2.36 Å, and the other three

(47) For simplicity, we define the Pt−Ru "bulk" values by considering the concentration-weighted average of Pt and Ru fcc lattice constants (so-called Vegard's rule), which just indicates a completely geometric expectation. However, we note that there are always deviations from Vegard's rule in any alloy system, i.e., positive (negative) deviation for segregating (ordering) type.

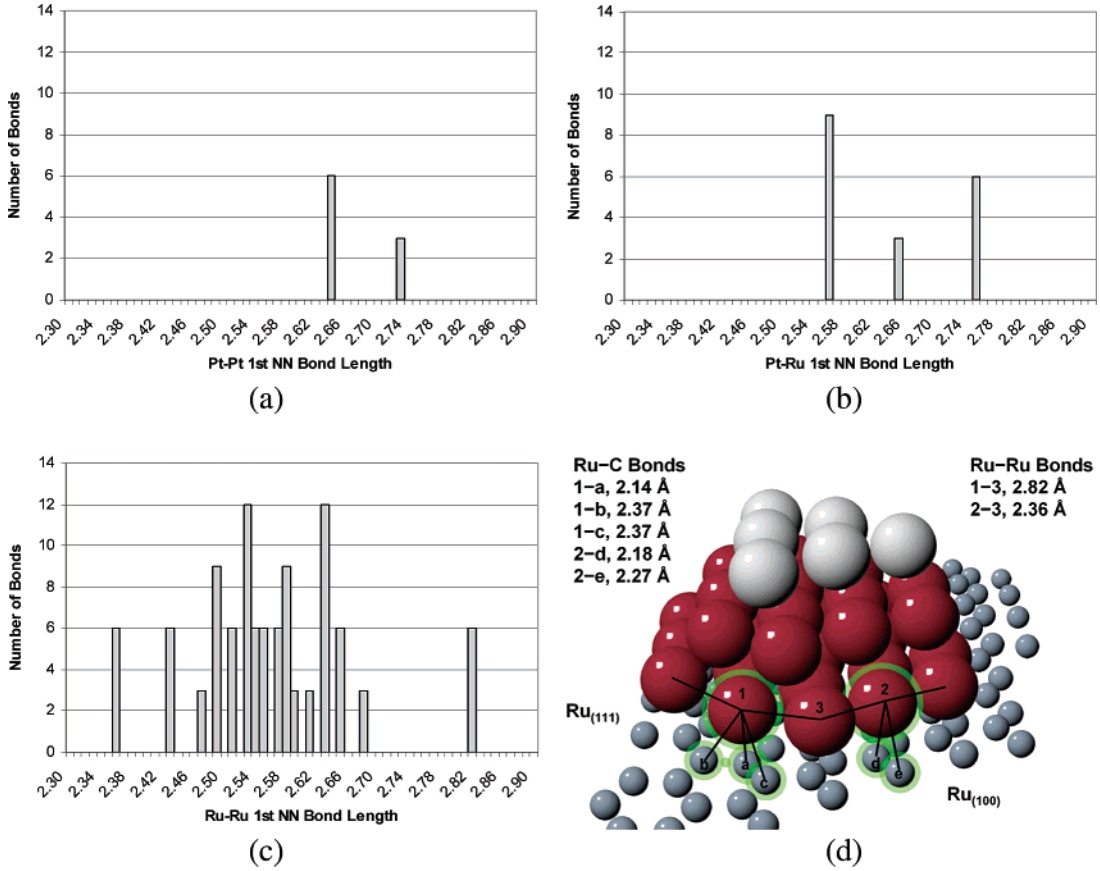

Figure 6. Distributions of first NN metal−metal bond length calculated with DFT−LDA for Pt_6Ru_{31} supported on a graphite: (a) Pt−Pt, (b) Pt−Ru, and (c) Ru−Ru. Average first NN bond lengths are 2.67, 2.64, and 2.56 Å for Pt−Pt, Pt−Ru, and Ru−Ru, respectively. Relaxed structure for the supported Pt_6Ru_{31} cluster is shown in part d. The legends for atoms are as in Figures 2 and 3. Metal−carbon and metal−metal bonds are drawn in black lines and listed as in Figure 4. The $Ru_{(111)}$, $Ru_{(100)}$ atoms and the closest C atoms to them are highlighted.

are 2.82 Å. In contrast, the Ru−Ru bond between two core Ru atoms in the central layer is 2.60 Å (not shown in the figure). Besides the effect of the interaction with the carbon support, it is well-known that a cluster has intrinsic static bond disorder due to the relaxation from the close packing, which has been confirmed by many studies.[48,49] In a perfect O_h cluster, due to symmetry, the surface bonds along the perimeter of the central hexagon are equivalent. When the Pt or Pt−Ru clusters form on a support, the cuboctahedron is truncated and the symmetry is lowered. The 3-fold rotational symmetry (with no inversion point) will make the six surface bonds in the bottom hexagonal layer inequivalent. This inequivalence can be enhanced when the cluster interacts with a graphite surface. This effect is much larger for Pt_6Ru_{31} than Pt_{37} cluster. For the former, the longer bonds get even larger (increasing to 2.82 Å) and the shorter bonds get smaller (decreasing to 2.36 Å). As seen in Figure 6d, the $Ru_{(111)}$ atoms move toward the hollow sites on the graphite and have lower positions in the *z* direction than the other atoms in the bottom layer. In contrast, the $Ru_{(100)}$ atoms move toward the bridge sites and do not change their positions in the *z* direction. The closest C atoms to the $Ru_{(111)}$ atom are at 2.14 Å and two at 2.37 Å, while those to the $Ru_{(100)}$ atom are at 2.18 Å and at 2.27 Å. The shorter Ru−C distances between $Ru_{(111)}$ and the hollow site than between $Ru_{(100)}$ and the bridge site show that the former is preferred.

Electronic Structures and Origin of Bond Disorder. The different binding of $M_{(111)}$ and $M_{(100)}$ with a graphite surface can be analyzed in the view of electronic structures. Figure 7 shows the iso-surfaces of electron density difference at ±0.05 e/Å^3 for the Pt_{37} and Pt_6Ru_{31} clusters supported on the graphite surface in parts a and b, respectively. The electron density difference is calculated by subtracting electron densities of the substrate and the clusters from the whole supported system with the same relaxed geometry. Most of the electron density redistribution upon adsorption happens in the metal−C interface. There is very little electron density redistribution around the top metal layer, which shows that the support effect diminishes in going away from the interface region. This is in agreement with the analysis of the intralayer buckling in the previous section. It is easy to see that Figure 7b has much more electron density redistribution than a. From this we see that the Ru−C interaction is much stronger than the Pt−C interaction, due to charge-transfer/bond enhancement, and agrees with the calculated adsorption distance being shorter for Ru−C than Pt−C.

In Figure 7b, around the Ru−C interface region, the electron density is depleted (shown in red) from the *d* type orbitals around the Ru atoms. In contrast, the electron density is accumulated (shown in yellow) mostly in the middle of the Ru−C interface region and right on top of the C atoms. These features show the strong interaction between Ru atoms in the bottom layer and the C substrate, most of which is the overlap between the Ru *d* orbitals and the C π orbitals pointing out of the

(48) Ankudinov, A. L.; Rehr, J. J.; Low, J. J.; Bare, S. R. *J. Chem. Phys.* **2002**, *116*, 1911−1919.
(49) Boyanov, B. I.; Morrison, T. I. *J. Phys. Chem.* **1996**, *100*, 16310−16317.

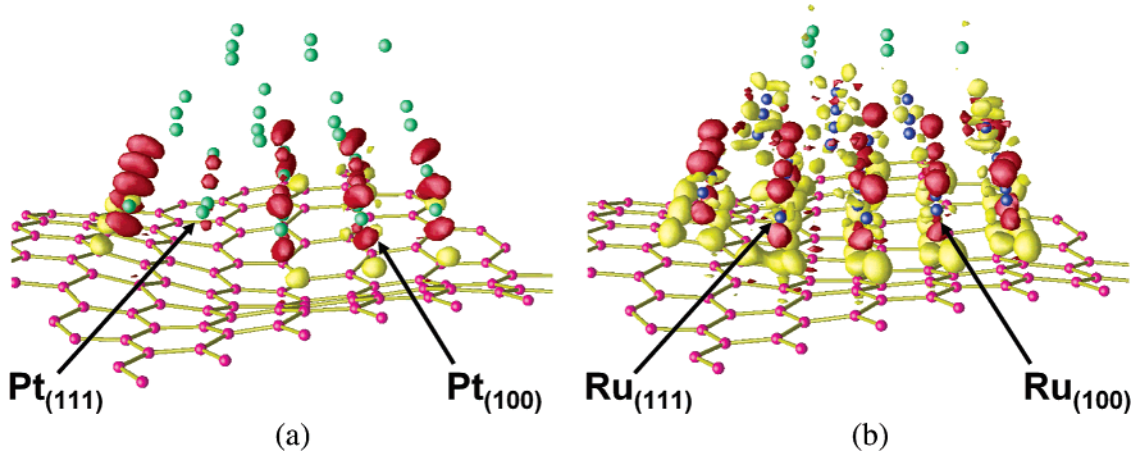

Figure 7. Electron density difference for (a) Pt_{37} and (b) Pt_6Ru_{31} clusters supported on a graphite surface. The value of the iso-surface is ±0.05 e/Å^3. Red stands for electron depletion and yellow for electron accumulation. Green, blue, and purple spheres stand for Pt, Ru, and C atoms, respectively.

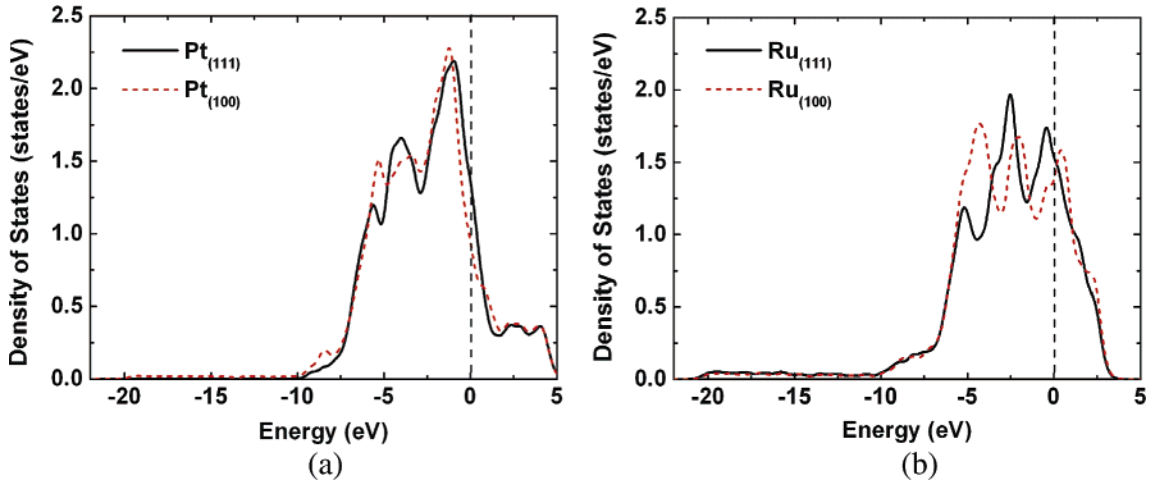

Figure 8. Projected density of states on (a) $Pt_{(111)}$ and $Pt_{(100)}$ atoms and (b) $Ru_{(111)}$ and $Ru_{(100)}$ atoms.

substrate. There are three lobes of electron density accumulation around each $Ru_{(111)}$ atom, which are the result of the interactions of the $Ru_{(111)}$ atoms with the three nearby C atoms around the hollow site. Around the $Ru_{(100)}$ atoms, there are only two lobes of electron density accumulation because they are only in close interaction with two C atoms crossing the bridge site. In contrast, as shown in Figure 7a, there is no electron density redistribution around the $Pt_{(111)}$ atoms and some around the $Pt_{(100)}$ atoms at the iso-surface value of ±0.05 e/Å^3 , which agrees with the observation that the $Pt_{(111)}$ atoms relax upward and away from the hollow site and no carbon atom is in close interaction with it, while the $Pt_{(100)}$ atoms have close interactions with the underlying carbon atoms. These features can also be seen in the Ru−C and Pt−C bond lengths in Figures 4b and 6d.

The difference in bonding environment can also be seen clearly in the projected density of states (PDOS) on the $M_{(111)}$ and $M_{(100)}$ atoms in Figure 8. Inside the supported 37-atom metal cluster, the $M_{(111)}$ atom has seven first NN, while $M_{(100)}$ atom has six first NN and two second NN. As seen in parts a and b of Figure 8, both $Pt_{(100)}$ and $Ru_{(100)}$ atoms have more states in a lower energy range than $Pt_{(111)}$ and $Ru_{(111)}$ atoms, respectively. This shows that the binding of the $M_{(100)}$ atoms inside the metal cluster is stronger than the $M_{(111)}$ atoms. From −20 to −10 eV, there is some overlap between Ru *s* and C π orbitals, while there is almost no such overlap between Pt *s* and C π orbitals. The C π orbitals lie mostly above −3 eV. In this energy range, see Figure 8b, there are more states from $Ru_{(111)}$ atoms than $Ru_{(100)}$ atoms, also indicating, as discussed above, that $Ru_{(111)}$ atoms form more Ru−C bonds than $Ru_{(100)}$ atoms. For the Pt_{37} cluster in this energy range, see Figure 8a, there are more states from $Pt_{(100)}$ atoms than $Pt_{(111)}$ atoms, confirming also that $Pt_{(100)}$ atoms form stronger Pt−C bonds than $Pt_{(111)}$ atoms. So the enhancement of bond length disorder is a consequence of anisotropic relaxation in different facets of the metal clusters and is enhanced by the different binding sites for the metal atoms in the bottom layer on the graphite surface.

Topology of Supported Bimetallic Clusters and Bond Counting. Several aspects of the results from detailed calculations warrant further explicit comment. Here, we point out that the tendencies toward segregation and the adoption of the close-packed structure can be explained in several ways, depending upon one's physical perspective. In a material science view, the phase segregation of Pt and Ru in bulk is predicted by the Hume−Rothery rules.[50] These largely empirical correlations predict patterns of solubility and compound formation in binary metallic systems based on considerations of atomic radii, bulk crystal structures, electron affinities (and ionization potential), and valency. These rules, of course, have an electronic origin, arising rigorously from electronic bandwidth differences of alloying elements, which affects such aspects as orbital overlap

(50) Hume−Rothery, W.; Smallman, R. E.; Haworth, C. W. *The Structure of Metals and Alloys*, 5th ed.; The Institute of Metals: London, U.K., 1969.

and band-filling.[51] For Pt and Ru binary alloys, the segregation effects experimentally appear to follow from the filling of unfavorable antibonding states in the Pt, which can be reduced by segregating this component, rather than from perturbations from the occupancy of the nonbonding states of the Ru. For example, using VASP we calculated the formation energy for an fcc(111) layer of Pt embedded between hcp(0001) or fcc-(111) layers of Ru, and for a fcc(111) layer Pt layer residing on the surface of the same hcp or fcc Ru. (For these calculations, we used 5 layers of Ru and 15 Å of vacuum with a k-point mesh of $20 \times 20 \times 1$.) The results reveal a strong energetic preference for the *surface-segregated* Pt structure over a *subsurface* Pt by 0.15 eV/(surface atom) for an hcp Ru and by 0.14 eV/(surface atom) for an fcc Ru surface. (Recall that subsurface Pt configuration is 4 eV higher for the supported nanocluster, or roughly 0.11 eV per cluster atom.) Clearly, Pt prefers sitting on the ambient surfaces of Ru, as expected from a simple band-filling argument.

With considerable accuracy, the identities of elements that will tend to enrich a surface in a binary (or higher) phase, or sit at the ambient surface in a metallic cluster, are predicted from the RCA gas tables,[52] developed for use in the design of vacuum tubes. In this analysis, whichever element has the lowest relative vapor pressure (a parameter correlated explicitly with its cohesive energy density) will be the one found to enrich the surface. These tables notably predict the segregation of Pt on Ru surfaces.

The final question that remains then is one related to the nanoparticle's structural motif. Why do the metal atoms in the bimetallic Pt−Ru clusters supported on carbon form a close-packed topology, rather than a planar one? In a trivial physical sense, this is the most energetically favorable coordination as it is one that is able to maintain more metallic electron density, i.e., it maximizes M−M bonds. A bond-counting argument can be made that mimics the calculated results extremely well. To do this, we performed EAM[53,54] energy minimization calculations, based on potentials from Johnson,[55] for a truncated cuboctahedral Pt_{37} cluster and hexagonal planar cluster of 37 Pt atoms on a Pt(111) surface with full cluster−substrate (strong metallic) interactions and with no cluster−substrate interactions (weak interactions to mimic carbon). These approximate, and significantly less intensive, calculations, which use an effective medium approach and embedding function derived from density-functional-type arguments, reproduce the cluster structure and bond lengths in reasonable agreement with VASP, although the energies obtained in this way are not as accurate.

Generally, for a hexagonal planar cluster residing on a Pt-(111) surface, there are 291 bonds generated (111 with substrate and 180 within cluster), while there are 261 bonds generated (57 with substrate and 204 within cluster) for the supported close-packed 3D cluster. The calculated results for the binding energies per cluster atom were 5.54 eV/atom for the hexagon with substrate interaction versus 4.40 eV/ atom without it (i.e., mimicking a weaker support interaction, as expected for carbon). For the cuboctahedral geometry, the corresponding numbers were 5.53 and 4.95 eV/atom, respectively. Not surprisingly, the lowest energy configurations found by EAM are for the strong metallic cluster-substrate cases, where the layered configuration is favored, but differences are less pronounced between close-packed and layered. However, for the case with no or little substrate interactions, the 3D structure clearly wins by ~0.6 eV/atom, as it produces more bonding in a metallic cluster.

This simply highlights that the structural habits seen in supported clusters will depend very sensitively on the electronic nature of those cluster−substrate interactions. Bonding that involves a more metallic substrate would promote the formation of cluster habits that are more layer-by-layer in nature (raft-like). Weaker interactions prefer, instead, topologically close-packed motifs of the metallic clusters. The oblate closed-packed shapes formed on carbon thus represent an intermediate case, and, as we have seen, the details of the interactions determine the cluster structure, bond distributions, and bond disorder, which have different origins for pure Pt and mixed Pt−Ru clusters on carbon.

Clearly, then, the control and modification of the support provides an interesting area on which to focus the development of new capacities for controlling nanoparticle structures and dynamics. An interesting possibility in the present context would be to modify the carbon-based support via intercalation of atoms such as Li to enhance pinning metallic clusters in an orderly arrangement, because the Li atoms order in a two-dimensional array due to electrostatic interaction. Such modifications will be examined in future theoretical investigations.

Conclusion

In conclusion, we have used DFT calculations to study truncated cuboctahedral homometallic Pt_{37} and bimetallic Pt_6Ru_{31} clusters supported on a graphite surface and provided insights into general expectations for bond length distributions and bond disorder in nanoclusters. We then used this as a guide to reinterpret the experimental EXAFS results. Segregation of Pt to the ambient surface in mixed clusters was explained electronically, which is also easily predicted by the RCA gas tables (which is probably more broadly applicable). As indicated by adsorption energies, bonding distance, and change in the electronic structures upon adsorption, the Ru−C interaction is found to be stronger than the Pt−C interaction, directly impacting cluster structure and electronic properties. For direct comparison with experiment, we studied metal−metal bonds in the supported clusters in detail. In agreement with our previously published EXAFS experiments,[7,11] we found that the metal−metal bonds in these two types of clusters are bulklike, while the bond length disorder is large due to a broad bimodal distribution for first NN metal−metal bonds. We determined the origin of the bond length disorder from an atom-by-atom structural analysis and showed that it results from anisotropic distortions in the cluster arising from interactions of the bottom metal layer in contact with the graphite surface. The details of the bond length disorder are distinctly different for the pure Pt and mixed, segregated Pt−Ru clusters due to the differing electronic nature of the mid- and late-transition-metal atoms, and the experimental data was reinterpreted. Such theoretically determined structural analysis can now be used to provide a

(51) Pinski, F. J.; Ginatempo, B.; Johnson, D. D.; Staunton, J. B.; Stocks, G. M.; Gyorffy, B. L. *Phys. Rev. Lett.* **1992**, *68*, 1962−1962.
(52) Honig, R. R.; Kramer, D. A. *RCA Review*; RCA Laboratories: Princeton, NJ, 1969.
(53) Daw, M. S.; Baskes, M. I. *Phys. Rev. B: Condens. Matter Mater. Phys.* **1984**, *29*, 6443−6453.
(54) Foiles, S. M.; Baskes, M. I.; Daw, M. S. *Phys. Rev. B: Condens. Matter Mater. Phys.* **1986**, *33*, 7983−7991.
(55) Johnson, R. A. *Phys. Rev. B: Condens. Matter* **1989**, *39*, 12554−12559.

structural model for the analysis of experimental data and provides a deeper insight into the details of structure and properties of supported metallic nanoclusters. Clearly, for supported catalytic clusters, the symmetry and type of support (strength of interface interactions with the clusters) will greatly affect the structural properties, which are the focus of our future work, namely, Pt clusters on different substrates, such as TiO_2, Al_2O_3, and BN.

Acknowledgment. This work was supported in part by the U.S. Department of Energy through the Frederick Seitz Materials Research Laboratory at the University of Illinois under Grants DE-FG02-91ER45439 and DE-FG02-03ER46026. L.L.W., D.D.J., and RN acknowledge support by the U.S. Department of Energy Catalysis Grant No. DE-FG02-03ER15476 and A.I.F. Grant No. DE-FG02-03ER15477. We also acknowledge critical computational support provided by the Materials Computation Center through National Science Foundation ITR Grant DMR-0325939 as well as the visitors program for V.C. during his stay in D.D.J.'s theory group.

JA053896M